Biochemistry

pubs.acs.org/biochemistry Article

Characterization of a Nitro-Forming Enzyme Involved in Fosfazinomycin Biosynthesis

Hannah Valentino and Pablo Sobrado*

Cite This: https://doi.org/10.1021/acs.biochem.1c00512 Read Online

ACCESS | Metrics & More | Article Recommendations | Supporting Information

ABSTRACT: *N*-hydroxylating monooxygenases (NMOs) are a subclass of flavin-dependent enzymes that hydroxylate nitrogen atoms. Recently, unique NMOs that perform multiple reactions on one substrate molecule have been identified. Fosfazinomycin M (FzmM) is one such NMO, forming nitrosuccinate from aspartate (Asp) in the fosfazinomycin biosynthetic pathway in some *Streptomyces* sp. This work details the biochemical and kinetic analysis of FzmM. Steady-state kinetic investigation shows that FzmM performs a coupled reaction with Asp (k_{cat}, 3.0 ± 0.01 s^{-1}) forming nitrosuccinate, which can be converted to fumarate and nitrite by the action of FzmL. FzmM displays a 70-fold higher k_{cat}/K_M value for NADPH compared to NADH and has a narrow optimal pH range (7.5−8.0). Contrary to other NMOs where the k_{red} is rate-limiting, FzmM exhibits a very fast k_{red} (50 ± 0.01 s^{-1} at 4 °C) with NADPH. NADPH binds at a K_D value of ∼400 μM, and hydride transfer occurs with *pro-R* stereochemistry. Oxidation of FzmM in the absence of Asp exhibits a spectrum with a shoulder at ∼370 nm, consistent with the formation of a C(4a)-hydroperoxyflavin intermediate, which decays into oxidized flavin and hydrogen peroxide at a rate 100-fold slower than the k_{cat}. This reaction is enhanced in the presence of Asp with a slightly faster k_{ox} than the k_{cat}, suggesting that flavin dehydration or Asp oxidation is partially rate limiting. Multiple sequence analyses of FzmM to NMOs identified conserved residues involved in flavin binding but not for NADPH. Additional sequence analysis to related monooxygenases suggests that FzmM shares sequence motifs absent in other NMOs.

INTRODUCTION

Flavin-dependent monooxygenases (FMOs) are a large family of enzymes known for their catalytic versatility.[1] FMOs are commonly found in natural product biosynthetic pathways, where they play a major role in the addition of functional groups essential for bioactivity.[1,2] This family has been categorized into eight classes, A−H, according to structural and mechanistic characteristics.[3] Our group has been studying several members of class B FMOs as these enzymes perform highly specific oxidations useful for biomedical and biotechnological applications.[4−9]

N-hydroxylating monooxygenases (NMOs) are members of class B FMOs that harness the redox power of the flavin cofactor to oxidize nitrogen atoms. Characterization of prokaryotic and eukaryotic NMOs involved in siderophore biosynthesis has provided a detailed description of their structure and mechanism of action.[5,10−17] In recent years, this family has expanded with the discovery of nitro-forming NMOs.[18−22] Nitro-containing compounds, such as nitroalkanes, are highly valued industrial chemicals due to their application as solvents and intermediates for organic synthesis of pharmaceutical drugs[23,24] with an annual production of over a million tons in the United States.[25] Nitro-synthesis depends on high temperatures and acidic conditions, resulting in large amounts of environmentally hazardous waste.[24] Because of this, there has been great interest in improving nitro-formation, including biosynthetic applications.[24,26−30] In addition to these methods, nitro-forming NMOs are potential candidates for biotechnological applications as an alternative to current nitro-synthesis techniques.

Fosfazinomycin M (FzmM) is a nitro-forming NMO that is involved in the biosynthesis of the natural products fosfazinomycin A and B (Scheme 1A) in some *Streptomyces* sp.[18] These compounds exhibit antifungal activity and contain a unique hydrazide core, which is an uncommon motif in natural products.[31−34] FzmM has been shown to play a role in hydrazide bond formation[18−20] by catalyzing the oxidation of L-aspartate (Asp) to nitrosuccinate (Scheme 1B). In the biosynthesis of cremeomycin, the FzmM homologue CreE has been shown to catalyze the same reaction.[22] Based on what has been reported for CreE and on nitrogen oxidation chemistry, the reaction of FzmM is believed to involve a six-electron oxidation on the primary amine of Asp, consuming three molecules of NADPH and oxygen to form nitrosuccinate (Scheme 1B).[21,30] In this work, we describe the kinetic characterization of the nitro-forming NMO FzmM providing a detailed report of its mechanism toward the formation of nitrosuccinate.

Received: July 30, 2021

https://doi.org/10.1021/acs.biochem.1c00512
Biochemistry XXXX, XXX, XXX−XXX

Scheme 1. (A) Structures of Fosfazinomycin A/B.[32] (B) FzmM Performs a Six Electron Oxidation on L-aspartate (Asp) with NADPH and Oxygen as Substrates to Produce Nitrosuccinate.[31] Nitrosuccinate is Then Converted to Nitrite and Fumarate by the Fumarase-like Enzyme FzmL.[18,30] The Nitrogen-Labeled Red Represents Nitrogen Incorporated into Fosfazinomycin A/B from the Nitrite of Asp

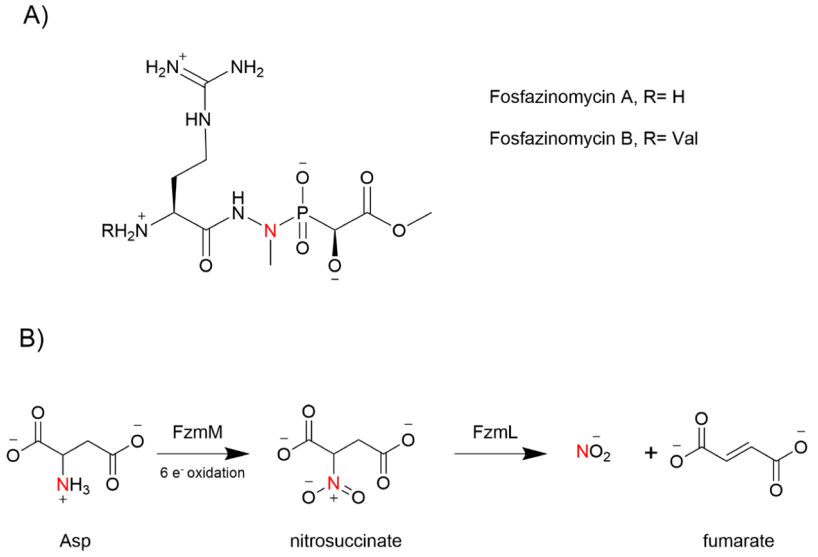

EXPERIMENTAL PROCEDURES

Materials. All substrates were purchased from Sigma-Aldrich (St. Louis, MO). NAD(P)H and NAD(P)$^+$ were purchased from Research Products International (Mt Prospect, IL), and deuterated nicotinamide phosphate (4*R*)-[4-^{2}H]-NADPD was synthesized following previously published protocols.[35] Protein BLUEstain ladder from GoldBio was used for sodium dodecyl sulphate−polyacrylamide gel electrophoresis (SDS-PAGE) gel analysis. Oneshot BL21 (DE3) *Escherichia coli* cells were purchased from Thermo Fisher Scientific (Waltham, MA) for protein expression. Codon-optimized genes coding for FzmM and FzmL (NCBI accession numbers: WP_053787792 and WP_053787793, respectively) were synthesized by GenScript (Piscataway, NJ). FzmM was subcloned into pET15b, and FzmL was subcloned into pET28a for *N*-terminal 6xHis tag expression.

FzmM Expression and Purification. Recombinant FzmM was expressed from a pET15b vector by IPTG induction. Transformed cells were grown in 50 mL of LB media supplemented with 0.1 mg/mL ampicillin overnight. Flasks[6] of 1 L LB media supplemented with ampicillin were inoculated with 8 mL of the pre-growth culture and shaken at 37 °C and 250 rpm until an optical density of 0.6 was obtained. Each flask was induced with 0.1 mM IPTG, the temperature lowered to 18 °C, and the cultures were shaken overnight. The cells were harvested by centrifugation at 5000*g* and stored at −70 °C.

Cell paste (∼40 g) was suspended by constant stirring at 4 °C into 150 mL of buffer A [50 mM potassium phosphate (pH 7.5), 300 mM NaCl, 20% glycerol, and 5 mM imidazole] supplemented with 1 mM phenyl methyl sulfonyl fluoride, 1 mg/mL lysozyme, 1 mg/mL DNase, and 1 mg/mL RNase. Cells were lysed by sonication, and the insoluble cellular content was separated from soluble lysate by centrifugation at 30,000*g* for 1 h at 4 °C. Three in-tandem 5 mL nickel-immobilized metal affinity chromatography (IMAC) columns were equilibrated with buffer A using an AKTA prime system (GE Healthcare, Chicago, IL). The supernatant was loaded onto the IMAC columns and washed with ∼40 mL of a mixture of 90% buffer A and 10% buffer B (50 mM potassium phosphate, pH 7.5, 300 mM NaCl, 20% glycerol, and 300 mM imidazole). The enzyme eluted at ∼180 mM imidazole using a combination of 40% buffer A and 60% buffer B. The fractions containing FzmM were pooled together and incubated with 50 μM FAD for 15 min on ice. The sample underwent buffer exchange into 100 mM potassium phosphate, pH 7.5, 10% glycerol, and 1 mM TCEP using an AKTA prime system equipped with a HiPrep 26/10 desalting column (Cytiva, Marlborough, MA). Protein was flash frozen in liquid nitrogen and stored at −70 °C.

FzmL Expression and Purification. Recombinant FzmL was expressed from a pET28a vector using an autoinduction method described previously.[4] Cell harvest and storage were the same as described above.

For purification of FzmL, buffer A was 25 mM HEPES, pH 7.5, 300 mM NaCl, and 10 mM imidazole and buffer B was 25 mM HEPES, pH 7.5, 300 mM NaCl, and 300 mM imidazole. Cells (∼20 g) were suspended in 150 mL buffer A. Cell lysis was performed, as described above for FzmM. Columns were washed with ∼40 mL of 30 mM imidazole (90% buffer A: 10% buffer B) before eluting the protein with 100% buffer B. Protein was buffer exchanged into 25 mM HEPES, pH 7.5, and 100 mM NaCl and flash frozen for long-term storage.

Oxygen Consumption. Enzyme activity was measured by following the consumption of oxygen using a Hansatech Clark-type oxygen electrode system (Amesbury, MA). The initial velocity was determined by measuring the slope of oxygen consumption within the first minute of reaction initiation. The total volume was 1 mL of 100 mM potassium phosphate, pH 7.5, and 10% glycerol. The reaction was initiated with 0.5 μM FzmM unless specified differently. The steady-state kinetic parameters were determined by measuring the initial velocities (v_0) of the reaction with varying concentrations of Asp (0.015−7.5 mM) with 1 mM NADPH or NAD(P)H (0.010−1 mM) with 15 mM Asp. The $v_0/[E]$ was plotted as a function of

https://doi.org/10.1021/acs.biochem.1c00512
Biochemistry XXXX, XXX, XXX−XXX

the substrate concentration and fit to the Michaelis−Menten equation (eq 1).

$$\frac{V_0}{[E]} = \frac{k_{cat}[S]}{K_M + [S]} \quad (1)$$

where k_{cat} denotes the reaction turnover number, K_M is the substrate concentration at half k_{cat}, $[E]$ is the total FzmM concentration, and $[S]$ is the concentration of the substrate. The molar equivalent of NADPH and Asp consumed was determined by measuring the rate and amount of oxygen consumed when 3 μM FzmM was reacted with 50 μM Asp and 50 (1 to 1), 100 (1 to 2), 150 (1 to 3), or 300 (1 to 6) μM NADPH.

Inhibition by $NADP^+$ was measured by varying concentrations of NADPH (0−1 mM) in the presence of 10 mM Asp at fixed concentrations of $NADP^+$ (0−1 mM). The data were analyzed by global analysis using the competitive inhibition model on GraphPad Prism (San Diego, CA) using eq 2. All variables are the same as defined in eq 1 with [I] representing the concentration of the inhibitor and K_i being its dissociation constant.

$$\frac{V_0}{[E]} = \frac{k_{cat}[S]}{(K_M\left(1 + \frac{[I]}{K_i}\right) + [S]} \quad (2)$$

The primary kinetic isotope effects (KIEs) using (4R)-[4-^{2}H]-NADPD was determined by measuring enzyme activity at varying concentrations (0−1 mM) in the presence of 10 mM Asp. The steady-state parameters were determined using eq 1. The ratio of steady-state kinetic variables with NADPH over the parameter NADPD was reported as the KIE.

Enzyme activity at different pHs was determined using the buffers [100 mM potassium phosphate with 10% glycerol (pH 6.0−7.5) and 100 mM Tris-Cl with 10% glycerol (pH 7.5−9.0)]. Assays were performed varying Asp (0.05−7.5 mM) at 1 mM NADPH. The data were analyzed using eq 1, and the determined k_{cat} and k_{cat}/K_M were plotted as a function of pH. Data that presented a curve with a single pK_a value were fit with eq 3 while those that exhibited a bell-shaped curve indicative of two pK_a values were fit with eq 4. The upper and lower pH limits of the curves are described as C and A, respectively.

$$\log(y) = \log\left(\frac{C + A(10^{(pK_a - pH)})}{1 + 10^{(pK_a - pH)}}\right) \quad (3)$$

$$\log(y) = \log\left(\frac{C}{1 + 10^{(pK_{a1} - pH)} + 10^{(pH - pK_{a2})}}\right) \quad (4)$$

Asp Consumption. The consumption of Asp was measured using fluorenylmethyloxycarbonyl chloride (FMOC-Cl) and 1-adamantylamine (ADAM) derivatization.[36] Assays were performed at a total volume of 100 μL with 1 μM FzmM, 1 mM Asp, and 5 mM NADPH and incubated at 25 °C with constant agitation. Time points were taken between 0 and 60 min. Aliquots of 30 μL of the reaction mixture were quenched with 200 μL of acetonitrile and the precipitant removed by centrifugation. A 130 μL volume of the quenched reaction was transferred and mixed with 25 μL of 0.2 M borate, pH 8.5. Derivatization was initiated with 3.4 μL of 150 mM FMOC-Cl prepared in acetonitrile, and the reaction was incubated for 5 min at room temperature. The reaction was quenched by the addition of 158 μL of 40 mM ADAM prepared in 50% acetonitrile. The assay was shaken (100 rpm) for 15 min and centrifuged before 10 μL of the sample was injected for separation, using a Phenomenex Luna 5 μm C18 column attached to a Shimadzu HPLC equipped with a photodiode array detector set to monitor the wavelength at 263 nm. Samples were eluted over a gradient of 20−100% buffer B for 50 min where buffer A was 0.1% trifluoroacetic acid (TFA) in HPLC grade water and buffer B was 0.1% TFA in acetonitrile. Consumption of Asp was measured using a standard curve from 0 to 1 mM Asp.

Nitrite Formation. Nitrite detection was accomplished using a Griess reagent kit (Invitrogen, Waltham, MA). A 1.5 mL of assay of 100 mM potassium phosphate (pH 7.5) and 10% glycerol containing 10 μM FzmL, 0.75 mM NADPH, and 5 mM Asp was initiated with 0.5 μM FzmM. Aliquots at a volume of 250 μL were taken at 5−120 min and quenched with 250 μL of 0.1 N HCl. The quenched sample was analyzed by mixing 150 μL of the sample with 20 μL of the Griess reagent and 130 μL of water on a 96-well plate and incubating for 30 min. The samples were measured at 548 nm using a SpectraMax M5 microplate reader (Molecular Devices, San Jose, CA). A standard curve was constructed with sodium nitrite and used to determine the nitrite concentration of the samples.

Hydrogen Peroxide Formation. To determine the rate of uncoupling of FzmM, reactions were performed at 0.5 μM FzmM, 10 mM Asp, and 1 mM NADPH in 100 mM potassium phosphate, pH 7.5, and 10% glycerol. Reactions were incubated for 1−10 min and quenched as per the instructions in the Pierce quantitative hydrogen peroxide kit (ThermoFisher). For detection, assays were transferred to a 96-well plate, and the absorbance at 562 nm was measured. A standard curve was constructed and used to determine the initial rate of hydrogen peroxide formation. The measurement of hydrogen peroxide formation using catalase was accomplished by comparing the rate of oxygen consumption of the enzyme under saturating conditions in the presence or absence of 1 mg/mL catalase.

Thermal Shift. SYPRO Orange dye was used to determine the thermal changes in FzmM and FzmL adapted from a previously reported procedure.[37] Assays were prepared in a Hard-Shell 96-well PCR plate (BioRad, Hercules, CA) mixing 2 μL of a 10× stock of fluorescent dye prepared from 5000× SYPRO Orange protein gel stain (ThermoFisher, Waltham, MA), 0.5 mg/mL of each enzyme, and select buffer to a final volume of 20 μL. To determine the change in the thermal shift when FzmM was reduced, 2 mM of NAD(P)H, 2 mM $NAD(P)^+$, 5 mM DT, or a combination of these was added to the reaction mix. To determine the effects of pH, 100 mM potassium phosphate with 10% glycerol (pH 6.0−7.5) and 100 mM Tris-Cl with 10% glycerol (pH 7.5−9.0) were used. A CFX qPCR system (BioRad) was programed to heat from 20 to 90 °C at a rate of 2 °C per minute. Changes in fluorescence were measured every 30 s using the FRET filter channel. The temperature of enzyme melting (T_m) was determined from the data collected using the Boltzmann equation described in a previous publication using GraphPad Prism.[37]

Stopped-Flow Spectrophotometry Assays. Stopped-flow assays were conducted using an SX20 stopped-flow spectrophotometer with a photodiode array detector from Applied Photophysics (Surrey, UK). Anaerobic conditions were obtained by storing the equipment inside a COY

https://doi.org/10.1021/acs.biochem.1c00512
Biochemistry XXXX, XXX, XXX−XXX

Table 1. Steady-State Kinetic Parameters of FzmM[a]

varying substrate	constant substrate	k_{cat}, s^{-1}	K_M, μM	k_{cat}/K_M, mM^{-1} s^{-1}	$^{D}k_{cat}$	$^{D}k_{cat}/K_M$
Asp	NADPH	3.0 ± 0.01	600 ± 50	5 ± 0.4	N.A.[b]	N.A.[b]
NADPH	Asp	3.3 ± 0.01	24 ± 0.5	140 ± 30	N.A.	N.A.
NADH	Asp	0.6 ± 0.04	300 ± 80	2 ± 0.5	N.A.	N.A.
(4*R*)-[4-^{2}H]NADPD	Asp	1.8 ± 0.05	22 ± 2	80 ± 8	1.7 ± 0.07	2 ± 0.4

[a]Conditions: 100 mM potassium phosphate (pH 7.5) and 10% glycerol with 10 mM Asp or 1 mM NADPH; the reported values are the mean and the errors are the standard deviation of four experiments. [b]N.A., not applicable.

Laboratories' (Grass Lake, MI) anaerobic chamber. Preparation of the sample handling unit, buffers, proteins, and substrate samples was accomplished following previously published methods.[38] Assays were performed in 100 mM potassium phosphate, pH 7.5, and 10% glycerol.

All assays studying the reductive half-reaction were measured at 4 °C using a water bath for temperature regulation. 7.5 μM FzmM was reacted with 0. 0.075−3 mM NADPH or 0.05−0.7 mM NADH (concentrations after mixing). Spectral changes from 190 to 850 nm were recorded on a logarithmic scale for 100 s or 300 s. The wavelength at 450 nm during reduction was fit with a single exponential decay (eq 5) when reacted with NADH and double exponential decay equation (eq 6) when reacted with NADPH. Changes that occurred to the reductive half-reaction in the presence of Asp were measured by adding 30 mM Asp to the NADPH solutions or incubating FzmM with 30 mM Asp prior to mixing.

The primary KIEs of the reductive half-reaction of FzmM were studied using isotopically labeled (4R)-[4-^{2}H]-NADPD. Anaerobically prepared enzyme was reacted with 2.5 mM of NADPD, and spectral changes were measured over 150 s. The absorbance changes at 450 nm were fit with double exponential decay (eq 6).

$$A_{nm} = A_1 e^{-k_{obs1}t} + C \quad (5)$$

$$A_{nm} = A_1 e^{-k_{obs1}t} + A_2 e^{-k_{obs2}t} + C \quad (6)$$

where A_{nm} is the absorbance at a specific wavelength, A_n is the amplitude of a specific phase, k_{obsn} is the observed rate of a specific phase, t is the time, and C is the final absorbance at the specific wavelength.

For the oxidative half-reaction, reduced enzyme solution was prepared by reacting 15 μM of FzmM with 15−20 μM NADPH. The reduced enzyme was reacted with 0−550 μM oxygen, and spectroscopic changes were recorded over 300 s. Reactions with the substrate were performed by mixing 20 mM Asp with oxygen or incubating it with reduced enzyme before mixing and measuring for 30 s. Absorbance changes at 370 and 450 nm were fit with a single exponential rise equation (eq 7).

$$A_{nm} = A_1(1 - e^{-k_{obs}t}) + D \quad (7)$$

where all the variables are defined the same as described for eqs 5−7 with the exception of D, which represents the initial absorbance value. Oxidation at varying concentrations of Asp was measured by reacting reduced enzyme with 300 μM O_2 mixed with Asp to a final concentration of 0−10 mM. Measurements were recorded for 150 or 30 s. Changes in absorbance at 370 nm and 450 nm were fit to eq 7.

The k_{obs} was plotted as a function of the substrate concentration. For data that exhibited a hyperbolic trend, eq 8 was applied.

$$k_{obs} = \frac{k_{max}[S]}{K_D + [S]} \quad (8)$$

where [S] is the substrate concentration, k_{max} is the maximum rate, and K_D is the dissociation constant of varying ligands. When k_{obs} was not dependent on the substrate concentration, the average of these values was reported. To determine the bimolecular rate constant of C(4a)-hydroperoxyflavin formation (k_{OOH}), the data were fit to a linear equation and the slope reported. For the slow phase of reduction and the oxidation at 450 nm, the observed rates did not change over substrate concentrations, and the average was reported.

Size-Exclusion Chromatography. The oligomeric states of FzmM and FzmL were determined using an AKTA prime plus FPLC. A High Prep 16/60 Sephacryl S-200 HR (GE Healthcare) column was equilibrated with 50 mM potassium phosphate, pH 7.5, and 100 mM NaCl at a flow rate of 1 mL/min. A standard curve consisted of ferritin (440 kDa), aldolase (160 kDa), conalbumin (75 kDa), and ovalbumin (43 kDa) from the high-molecular-weight marker kit (GE Healthcare) supplemented with tobacco etch virus protease (27 kDa) and RNase (13 kDa) (Sigma-Aldrich). A 500 μL of the enzyme sample at a final concentration of 1 mg/mL was passed through a 0.22 μM filter and injected onto the column. For samples where FzmM and FzmL were combined or contain 10 mM Asp, there was a 15 min incubation period on ice prior to the injection.

A standard curve was constructed by calculating the V_{av} of each standard's retention time using eq 9 where V_e is the elution volume of the sample, V_0 is the retention time of the void sample (blue dextrin), and V_T is the total column volume.

$$V_{av} = \frac{(V_e - V_0)}{(V_T - V_0)} \quad (9)$$

These values were plotted against log (MW) and used to determine the apparent molecular weight of the unknown sample using its elution volume. Protein containing fractions were collected and analyzed by 12% acrylamide SDS-PAGE.

RESULTS

Protein Expression and Purification. Recombinant FzmM and FzmL were expressed as *N*-terminus 6xHis-fusion proteins (in pET15b and pET28a, respectively) and purified using IMAC to >95% homogeneity, as determined by SDS-PAGE (Figures S1 and S2). The protein yield for FzmM was 1 ± 0.3 mg protein per 1 g of the cell pellet and had an FAD incorporation of 50 ± 4% (Figure S3). The extinction coefficient of FAD bound to FzmM at pH 7.5 is 13.5 mM^{-1} cm^{-1} at 450 nm. FzmL was purified at a yield of 10 ± 1 mg per 1 g of the cell pellet.

Steady-State Kinetics. FzmM exhibited activity with Asp with a k_{cat} of 3.0 ± 0.01 s^{-1} and a K_M of 600 ± 50 μM when NADPH was used as the substrate (Table 1 and Figure 1A).

https://doi.org/10.1021/acs.biochem.1c00512
Biochemistry XXXX, XXX, XXX−XXX

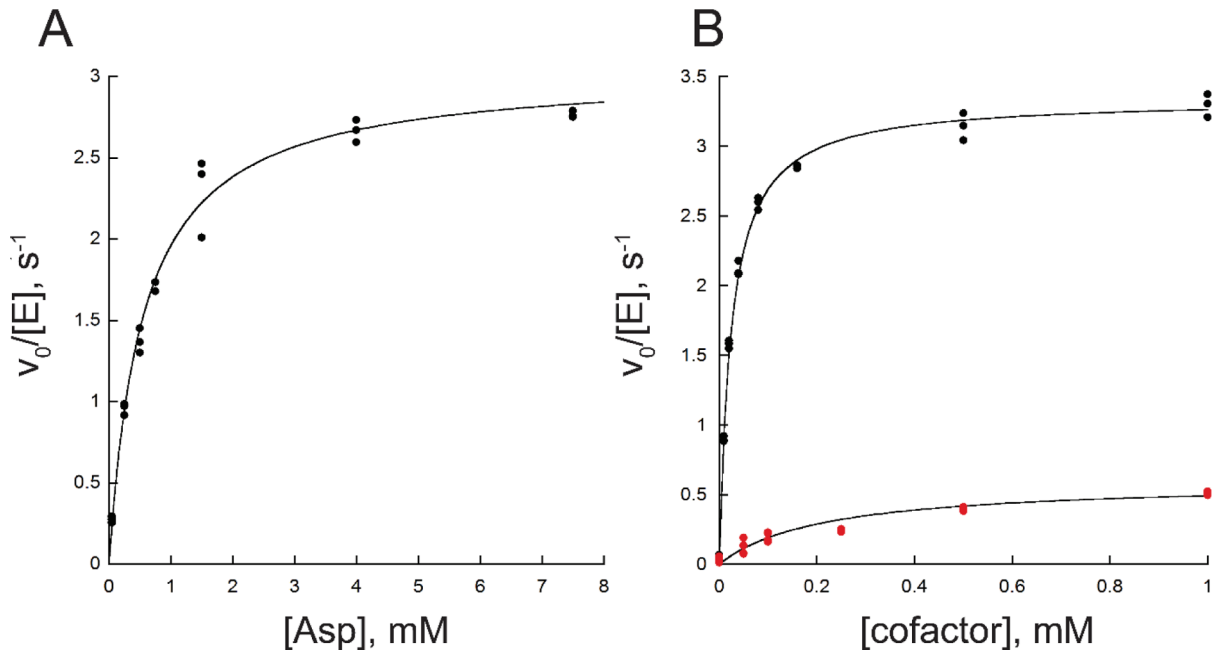

Figure 1. FzmM steady-state activity. (A) Initial activity of FzmM at increasing concentrations of Asp. (B) Initial activity of FzmM at increasing concentrations of NADPH (black) and NADH (red).

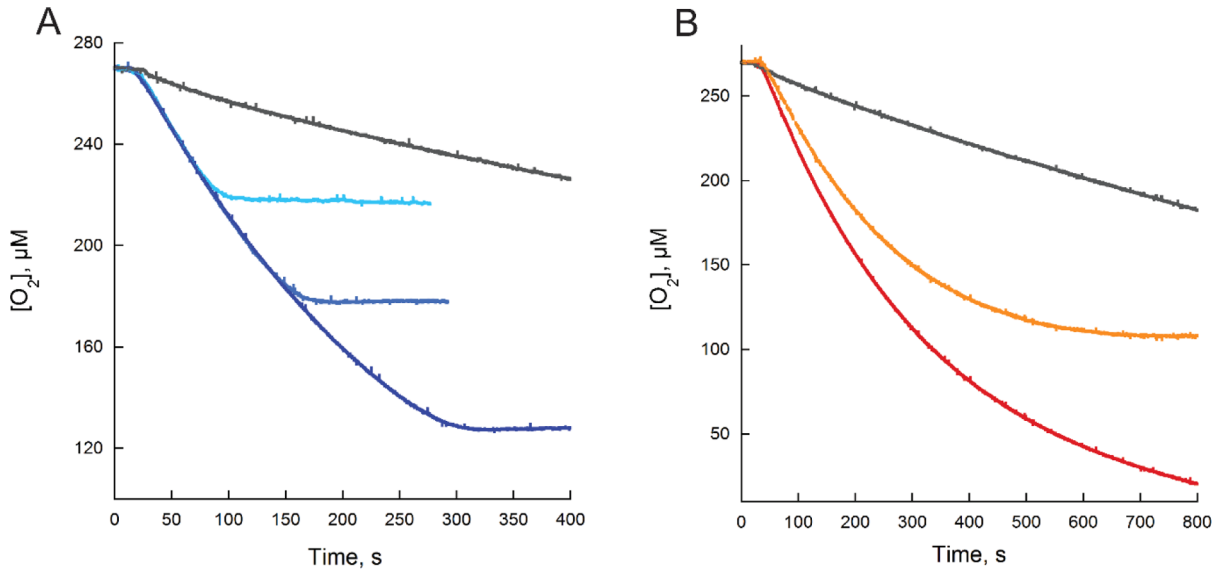

Figure 2. Change in the oxygen consumption of 3 μM FzmM at different concentrations of NADPH. (A) Enzyme reaction at 150 μM NADPH and no Asp (gray), 50 μM Asp and 50 μM NADPH (light blue), 50 μM Asp and 100 μM NADPH (blue), and 50 μM Asp and 150 μM NADPH (dark blue). (B) Enzyme reaction with 300 μM NADPH and no Asp (gray), 50 μM Asp and 300 μM NADPH (red), and the amount of oxygen consumed at 50 μM Asp and 300 μM NADPH when activity with no Asp is subtracted (orange). The total consumed oxygen for reactions was 52 ± 3 μM (light blue), 107 ± 8 μM (blue), 153 ± 9 μM (dark blue), and 150 ± 20 μM (orange).

When the potential substrates L-glycine, L-alanine, L-glutamate, L-asparagine, L-glutamine, and L-leucine were tested at 10 mM concentration, no activity above background was observed (Figure S4A). Similarly, the observed activity with Asp at 1 mM was not reduced when 10 mM of these compounds was present, suggesting that the tested substrates did not bind FzmM or that the K_D values were much higher than that for Asp (Figure S4B). Since oxygen consumption can occur without product formation (e.g., uncoupled reaction forming hydrogen peroxide), the consumption of Asp was monitored, and a decrease in the Asp concentration was observed under the same conditions (Figure S5). In addition, when this reaction was performed in the presence of FzmL, nitrite formation was detected (Figure S6). Multiple turnovers were confirmed by reacting 50 μM Asp with up to a three-molar equivalent of NADPH (Figure 2A). When a ratio of 1:6 Asp:NADPH was tested, oxygen was rapidly consumed up to 3 mol NADPH followed by an uncoupled reaction (Figure 2B). These results are consistent with FzmM performing multiple reactions on a single substrate molecule consuming 3 mol of NADPH and 3 mol oxygen for 1 mol Asp.

The catalytic efficiency with NADPH is ~70-fold higher than that for NADH, originating mainly from a 12-fold lower K_M value and a 5-fold higher k_{cat} value for NADPH (Table 1;

https://doi.org/10.1021/acs.biochem.1c00512
Biochemistry XXXX, XXX, XXX−XXX

Figure 1B). Product inhibition studies with $NADP^+$ show that the oxidized product is a competitive inhibitor versus NADPH with a K_i value of 70 ± 4 μM (Figure 3). The stereospecificity of the hydride transfer step was studied by measuring the primary KIEs with (4R)-[4-^{2}H]-NADPD on the steady-state parameters, and a KIE value on k_{cat} ($^Dk_{cat}$) of 1.7 ± 0.07 and 2 ± 0.4 for $^D(k_{cat}/K_M)$ was observed (Figure 4A; Table 1). These results show that flavin reduction is partially rate limiting in the catalytic cycle and that the reaction proceeds with a *pro*-R stereospecificity.

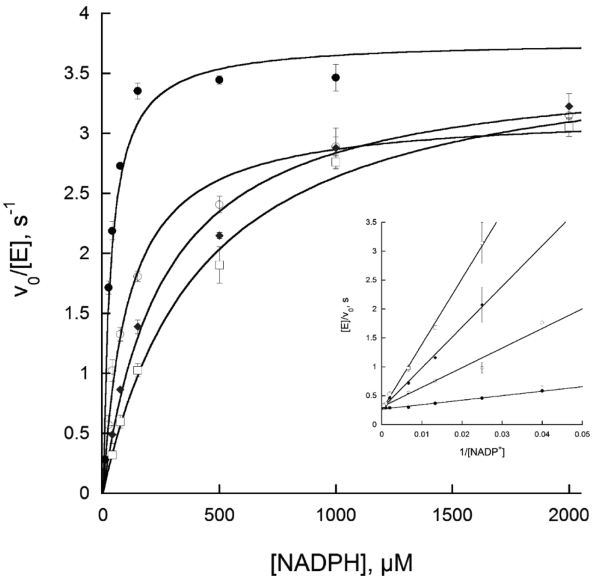

Figure 3. Inhibition of FzmM by $NADP^+$. Initial velocities of FzmM at increasing concentrations of NADPH in the presence of 0 mM (●), 0.25 mM (○), 0.5 mM (◆), and 1 mM (□) $NADP^+$ in 100 mM potassium phosphate, pH 7.5, and 10% glycerol. Inset, the double-reciprocal plot showing a *y*-intercept consistent with a competitive inhibition mechanism by $NADP^+$. The K_i was determined to be 70 ± 4 μM using the competitive inhibitor model on the GraphPad Prism (eq 2). The reported error is the standard deviation of three experiments.

Hydrogen Peroxide Formation. The activity of some FMOs can be uncoupled, meaning that instead of formation of a hydroxylated product, hydrogen peroxide is produced. Thus, to determine whether the reaction of FzmM is uncoupled, we measured the formation of hydrogen peroxide at saturating concentrations of NAD(P)H and Asp (Figure 5). From this experiment, it was determined that the reaction was only 3% uncoupled with NADPH and 25% with NADH. Similar results were observed when continuous hydrogen peroxide detection with catalase was performed (data not shown). It is worth noticing that when Asp is not under saturating conditions, higher uncoupling is observed (Figure S6).

Reductive Half-Reaction. Stopped-flow spectrophotometry was used under anaerobic conditions to determine the kinetic parameters of the reaction of FzmM with NAD(P)H (referred to as the reductive half-reaction) (Table 2). The reaction with NADPH resulted in bleaching of the peak at 450 nm in a biphasic process that occurred with a fast ($k_{fast,NADPH}$) and slow phase ($k_{slow,NADPH}$) (Figure 6). The majority of the change in absorbance occurred in the fast phase consisting of ~85% of the amplitude change. The fast phase at 4 °C was 17-fold larger than the k_{cat} at room temperature and was dependent on the NADPH concentration with a K_D value of 440 ± 30 μM. Performing this reaction in the presence of Asp slightly increased k_{fast} with no significant differences whether Asp was mixed with NADPH (Table 2, Asp) or incubated with the enzyme (Table 2, Asp*). The slow phase of the reaction remained constant at the various NADPH concentrations, was

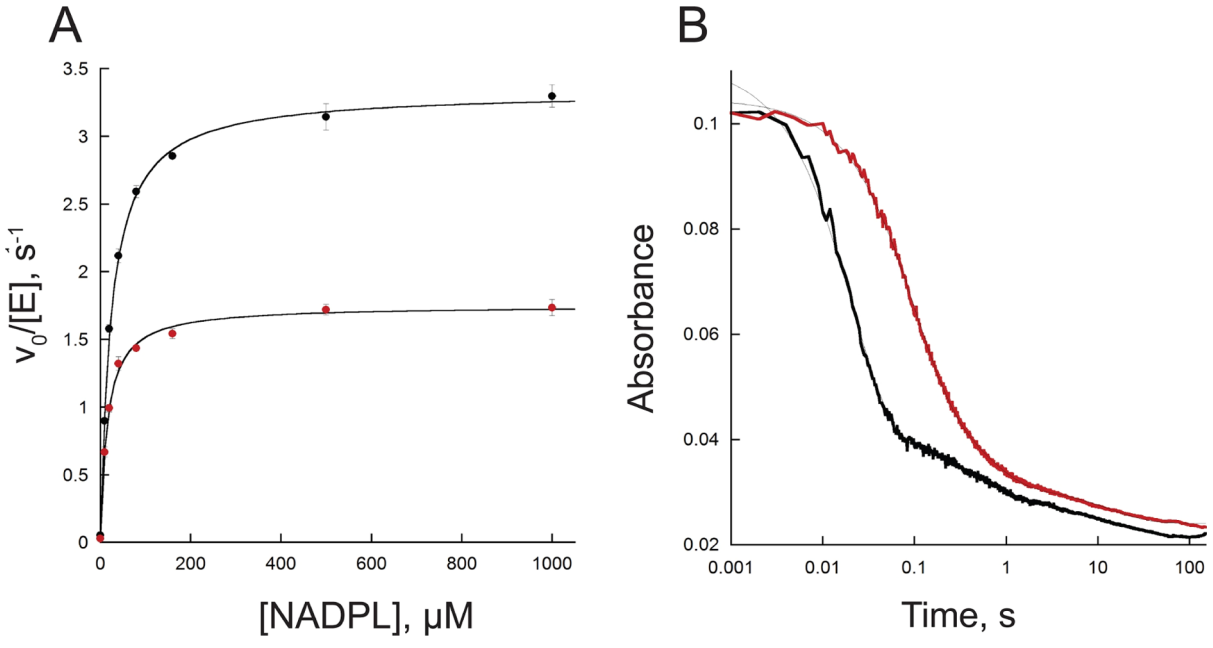

Figure 4. KIEs on steady-state kinetics and reductive half-reaction of FzmM. (A) Initial velocity of FzmM at varying concentrations of NADPH (black) or (4R)-[4-^{2}H]-NADPD (red). The value and error bars are the mean and standard deviation of three different experiments. (B) Observed rate of enzyme reduction at 450 nm at 2.5 mM NADPH (black) or (4R)-[4-^{2}H]-NADPD (red). NADPL represents the concentration of NADPH and (4R)-[4-^{2}H]-NADPD.

https://doi.org/10.1021/acs.biochem.1c00512
Biochemistry XXXX, XXX, XXX−XXX

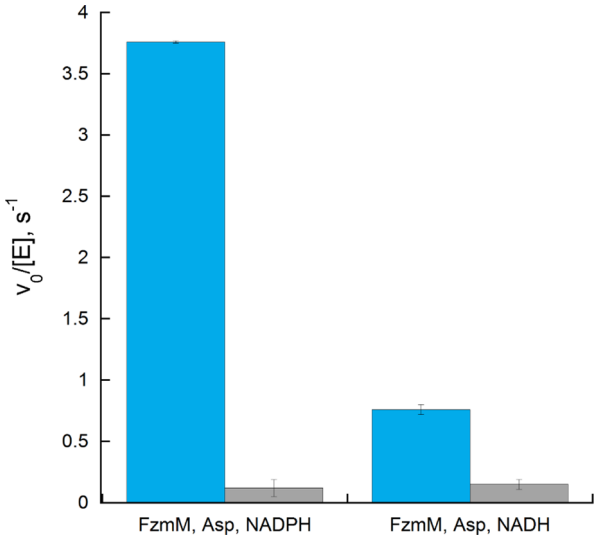

Figure 5. Initial velocity of oxygen consumption (blue) compared to the initial velocity of hydrogen peroxide formation (gray) under saturating conditions. Assays were performed with 0.5 μM FzmM, 10 mM Asp, 0.5 mM NADPH, or 1 mM NADH in 100 mM potassium phosphate, pH 7.5, and 10% glycerol. The rates of oxygen consumption were 3.8 ± 0.01 s^{-1} (NADPH) and 0.8 ± 0.04 s^{-1} (NADH), and the rates of hydrogen peroxide formation were 0.1 ± 0.01 s^{-1} (NADPH) and 0.2 ± 0.02 s^{-1} (NADH). The values are the mean and the errors are the standard deviation of three experiments.

present with or without Asp, and corresponded to the 10−15% amplitude change. This slow phase might be related to enzyme that was damaged in the degassing process. With NADH, in the absence of Asp, a single phased reaction was measured. The rate constant of reduction with NADH (apparent $k_{red\text{-}app,NADH}$) was much slower than the k_{fast} and $k_{fast,NADPH}$, and the apparent K_D value was higher (Figure S7 and Table 2). The stereochemistry of hydride transfer was probed by measuring the KIE on the reductive half-reaction with deuterated (4R)-[4-^{2}H]-NADPD. The KIE on the k_{fast} ($^Dk_{fast}$) was 5 ± 0.1, confirming *pro*-R stereospecific hydride transfer (Figure 4B and Table S1).

Oxidative Half-Reaction. The oxidative half-reaction (FzmM reduced by NADPH reacted with molecular oxygen) was also studied using stopped-flow spectrophotometry. The early time points showed a shoulder at ∼370 nm consistent with the formation of a C(4a)-hydroperoxyflavin intermediate (Figure 7). This shoulder was only well-defined when no Asp was present and decayed into oxidized flavin after ∼10 s. The rate constant of formation of this intermediate (k_{OOH}) was very fast, dependent on the oxygen concentration, and enhanced in the presence of Asp (Table 2 and Figure S8). In the absence of Asp, the rate constant of oxidation, which reports intermediate decay through H_2O_2 elimination ($k_{H_2O_2}$), was over 130-fold slower than the reaction k_{cat} and remained unchanged with increasing concentrations of oxygen (Figure S9). The reaction with Asp, representing flavin dehydration after Asp hydroxylation (k_{OX}), did not increase much as a function of the oxygen concentration (Figure S8). When the concentration of oxygen was kept constant and the concentration of Asp varied, the observed rate at 450 nm increased with a $K_{D,Asp}$ being 7 ± 0.3 mM (Figure S9). At the lowest tested concentration of Asp, the observed rate at 370 nm was already enhanced compared to the reaction without substrate and remained unchanged with increasing concentrations of Asp (not shown).

Determination of the Oligomeric State. Size-exclusion chromatography (SEC) was used to determine the oligomeric states of recombinant FzmM (predicted mass 68.9 kDa) and FzmL (predicted mass, 50.9 kDa). From these experiments, it was determined that the apparent molecular weight of FzmM is 60 ± 4 kDa and FzmL is 250 ± 10 kDa (Figure S10 and Table S2). These masses correlate to FzmM existing as a monomer and FzmL as a pentamer in solution. When these enzymes were incubated together prior to sample loading, no changes to the peak retention times were detected, and both proteins eluted separately (Figure S10B). There was no difference when the same experiment was repeated in the presence of Asp (data not shown).

Thermal Shift Experiments. The melting temperature (T_M) of FzmM and FzmL was determined under varying buffer conditions by measuring changes in relative fluorescence using SYPRO orange dye. From this experiment, it was determined that FzmM exhibits a T_M of 37.5 ± 0.2 °C and FzmL exhibits a T_M of 68.1 ± 0.02 °C under standard conditions (100 mM potassium phosphate, pH 7.5, and 10% glycerol). When the T_M value of FzmM was calculated in the presence of FzmL, the Tm value was unchanged (∼37.0 °C), similarly the Tm for FzmL did not significantly change in the presence of FzmM (∼68 °C) (not shown). The stabilization of FzmM in the presence of NADPH, NADH, NAD^+, and sodium dithionite (DT) was evaluated (Figure S11). These experiments showed that $NADP^+$ stabilizes FzmM; however, flavin reduction provides further stabilization since NADPH exhibits the highest increase in thermal stability.

Table 2. Rapid-Reaction Kinetic Parameters of FzmM[a]

kinetic constant	no Asp	Asp	Asp*
$k_{fast,NADPH}$, s^{-1}	50 ± 1	60 ± 2	59 ± 0.2
$k_{slow,NADPH}$, s^{-1}	0.6 ± 0.01	0.7 ± 0.1	0.2 ± 0.04
$K_{D,NADPH}$, μM	400 ± 30	400 ± 30	450 ± 3
$k_{red\text{-}app,NADH}$, s−1	0.2 ± 0.002	N.A.[b]	N.A.
$K_{D\text{-}app,NADH}$, μM	900 ± 10	N.A.	N.A.
k_{OOH}, M^{-1} s^{-1}	50,000 ± 5,000	70,000 ± 4,000	100,000 ± 10,000
k_{H2O2}, s^{-1}	0.03 ± 0.002	N.A.	N.A.
k_{OX}, s^{-1}	N.A.	5 ± 0.5	4 ± 0.7
$K_{D,Aspartate}$, mM	N.A.	7 ± 0.3	N.A.

[a]Conditions: 100 mM potassium phosphate, pH 7.5, and 10% glycerol at 4 °C in the absence of Asp (no Asp), mixed with 10 mM Asp (Asp), or incubated with 10 mM Asp (Asp*); the values are the mean and the errors are the standard deviation of four experimental replicates. [b]N.A., not applicable.

https://doi.org/10.1021/acs.biochem.1c00512
Biochemistry XXXX, XXX, XXX−XXX

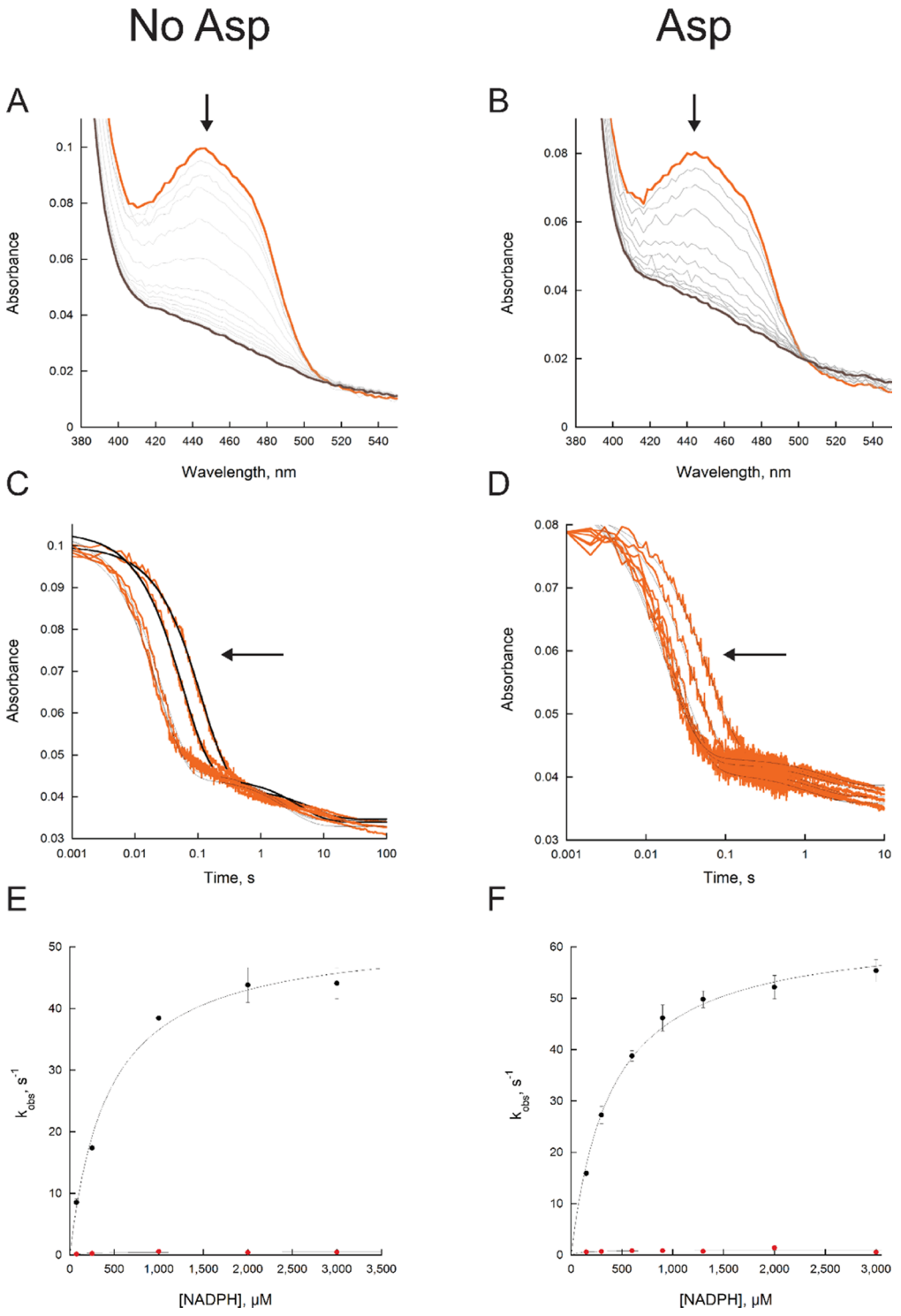

Figure 6. FzmM reduction with and without Asp. (A) Spectral changes in FzmM reacted with 150 μM NADPH without Asp from 380 to 600 nm over 180 s. (B) Spectral changes in FzmM reacted with 75 μM NADPH with Asp from 380 to 600 nm over 100 s. Reduced flavin is depicted in brown, and oxidized flavin is depicted in orange. (C) Changes in absorbance of FzmM at 450 nm without Asp at increasing concentrations of NADPH (0.1−3 mM) (orange). (D) Changes in absorbance of FzmM at 450 nm with Asp at increasing concentrations of NADPH (0.1−3 mM). Changes in panel (C,D) were fitted with double exponential decay (eq 6). (E) Observed rate of reduction at 450 nm without Asp at increasing concentrations of NADPH for the fast (black) and slow phase (red). (F) Observed rate of reduction at 450 nm with Asp at increasing concentrations of NADPH for the fast (black) and slow phase (red).

pH Effects. The steady-state kinetic parameters were measured as a function of pH, and changes to the k_{cat} and k_{cat}/K_M values were calculated (Table 3; Figure S12). From this experiment, the k_{cat} of FzmM is shown to be influenced by pH, exhibiting a short optimal range of 7.5−8.0 with a decrease at low and high pH values. Analysis of the pH profile shows that there is a group that is required to be deprotonated with a pK_a value of 6.8 ± 0.01 and another that needs to be

https://doi.org/10.1021/acs.biochem.1c00512
Biochemistry XXXX, XXX, XXX−XXX

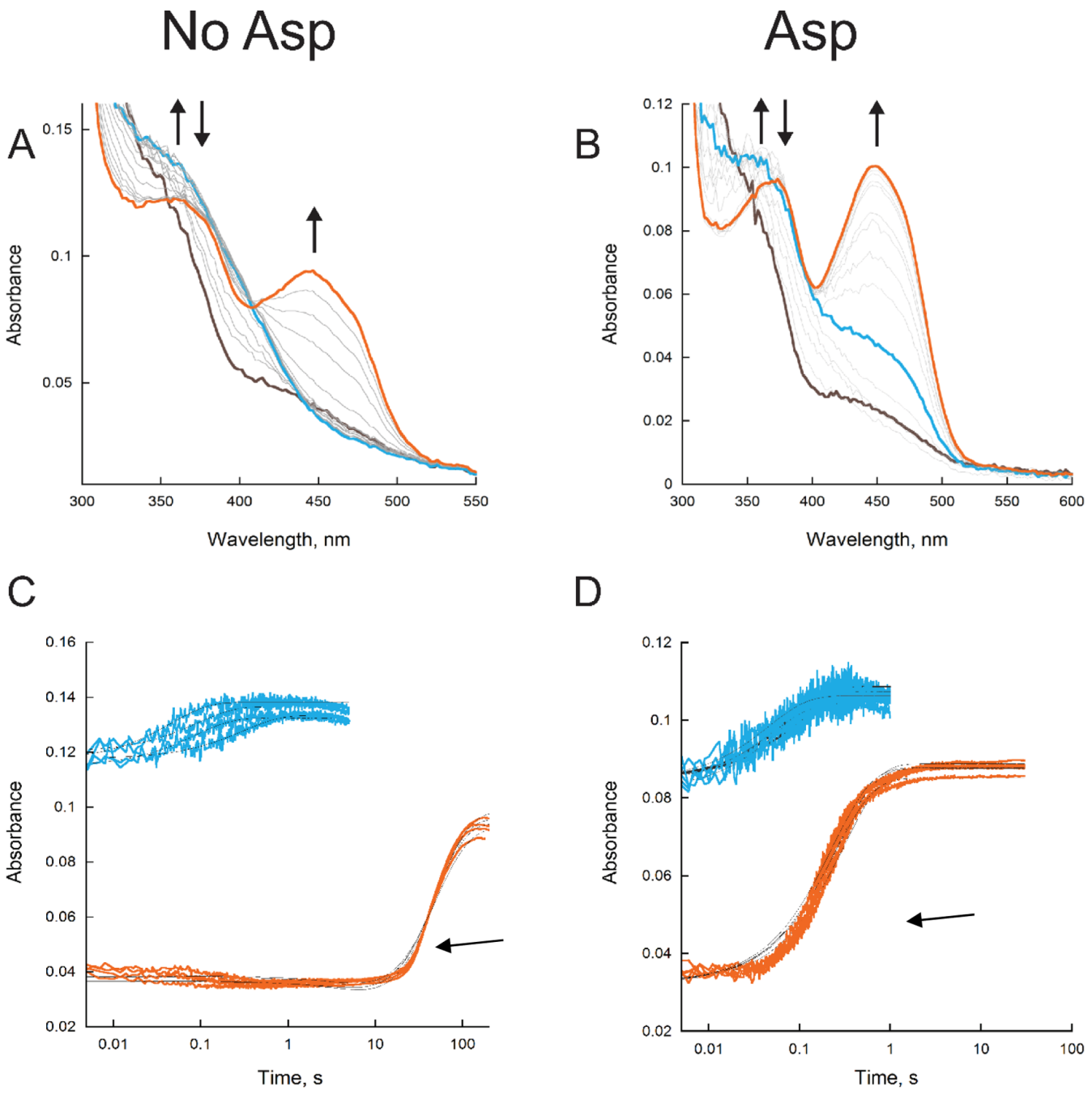

Figure 7. Sample of FzmM oxidation with and without Asp. (A) Spectral changes in reduced FzmM reacted with 250 μM O_2 from 300 to 700 nm over 100 s. (B) Spectral changes in reduced FzmM incubated with Asp reacted with 250 μM O_2 from 300 to 700 nm over 60 s. Reduced flavin is depicted in brown, the experimental C(4a)-hydroperoxyflavin intermediate is shown in blue, and oxidized flavin is shown in orange. Because of the rapid reaction with Asp, the increase in absorbance at 450 nm with the C(4a)-hydroperoxyflavin intermediate shown in panel B is expected to be oxidized enzyme. (C) Changes in absorbance of the FzmM reaction with oxidation in the absence of Asp at 370 nm (blue) fit with a single exponential rise equation, 450 nm (orange) fit with a double exponential rise equation. (D) Changes in absorbance of the FzmM reaction with oxidation with Asp at 370 nm (blue) fit with a single exponential rise equation and at 450 nm (orange) fit with a single exponential rise equation (eq 7). Both panels C and D depict traces at increasing concentrations of oxygen.

protonated with a pK_a value of 8.7 ± 0.02 (Figure S12A). The catalytic efficiency exhibits an upward rise from pH 6.0 to 7.5 before plateauing. This profile is consistent with a group that needs to be deprotonated for activity with a pK_a value of 7.3 ± 0.04 (Figure S12B). The effect of pH on FzmM stability was explored by measuring the T_M of the enzyme under buffers ranging from a pH of 6.0 to 9.0 (Figure S12C). The T_M of the protein remained unchanged in a pH range of 7.0−9.0. At a pH lower than 7.0, however, FzmM became increasingly less stable with a T_M of 31.6 ± 0.5 °C at pH 6.0.

DISCUSSION

NMOs have been under investigation for many years with the best characterized examples being the L-ornithine monooxygenases SidA from *Aspergillus fumigatus* and PvdA from *Pseudomonas aeruginosa*.[5,13−17,39−46] These enzymes perform a

https://doi.org/10.1021/acs.biochem.1c00512
Biochemistry XXXX, XXX, XXX−XXX

Table 3. pK_a Values—The Reported Error is the Standard Deviation of Four Experiments[a]

kinetic constant	pK_{a1}	pK_{a2}
k_{cat}	6.8 ± 0.01	8.7 ± 0.02
k_{cat}/K_M	7.3 ± 0.04	N.A.[b]

[a]Conditions: 100 mM potassium phosphate (pH 6.0−7.5) and 10% glycerol or 100 mM Tris-Cl (pH 7.5−9.0) and 10% glycerol. [b]N.A., not applicable.

single hydroxylation of the N-atom on the side chain of L-ornithine forming hydroxylamine, which is part of the hydroxamate moiety of siderophores. Despite their prevalence in natural product pathways, little is known about NMOs outside of siderophore biosynthesis.[13] Here, we present a detailed kinetic study of a nitro-forming NMO involved in fosfazinomycin biosynthesis. Because SidA is the NMO prototype, we will compare our results to those from SidA studies.

FzmM exhibits a highly coupled and specific reaction, with Asp and NADPH as its preferred substrates. When this reaction is performed in the presence of FzmL, nitrite formation is detected. These results are consistent with Asp undergoing multiple oxidations by FzmM forming nitro-succinate, which is cleaved into nitrite and fumarate by FzmL (Scheme 1B). This is consistent with a previous report.[18] The specificity of the reaction resembles that of SidA, which performs a coupled reaction with L-ornithine and NADPH.[4,12] Additionally, no activity was measured when different substrates were tested. The pH studies on the steady-state activity of FzmM describe a very narrow range of optimal pH (Figure S12).

It has been shown with SidA, and other NMOs, that the reductive half-reaction is the slowest step of the overall catalytic cycle.[13,15,40−42] However, the k_{red} is ∼100 times faster in FzmM with NADPH compared to SidA despite having a ∼500-fold higher K_D value (Table 2) (kinetic values of SidA are k_{red} 0.6 s^{-1} and K_D ∼ 1 μM).[42] FzmM shows a preference for NADPH as the k_{red} is at least ∼250-fold faster than that with NADH. Measurements of T_M show that when FzmM is reduced with NADPH or DT supplemented with $NADP^+$, there is an ∼4 °C positive shift (Figure 7). This shift only occurs with NADP(H), further confirming the specificity for this substrate. These data also suggest that the interactions between FzmM and the 2′ phosphate on the ribose sugar of NADP(H) trigger a conformational change that likely brings the nicotinamide closer to the active site facilitating the fast reduction reaction and stabilization of the C(4a)-hydroperoxyflavin. Oxidation follows a canonical class B FMO mechanism that requires the formation and stabilization of a C(4a)-hydroperoxyflavin intermediate. In the presence of Asp, intermediate formation is enhanced 2-fold and, at air saturated conditions, flavin oxidation occurs at a rate roughly similar to the k_{cat}. Thus, oxidation of Asp or dehydration of the hydroxyflavin is likely, at least partially, rate limiting in the catalytic cycle. $NADP^+$ was shown to be a competitive inhibitor of NADPH, indicating that it binds to oxidized FzmM and, therefore, is the last product to leave the active site. These features are common of a class B FMO mechanism (Scheme 2). The catalytic cycle of FzmM is initiated by the binding of NADPH, which rapidly transfers the *pro*-R hydride on the nicotinamide ring to the N(5) position of the flavin, reducing it to a flavin hydroquinone (Scheme 2A−C). The reduced flavin then reacts with oxygen forming a C(4a)-hydroperoxyflavin intermediate that is stabilized by $NADP^+$(Scheme 2D). In the absence of Asp, this intermediate slowly decays into hydrogen peroxide as part of an uncoupled reaction. In the presence of Asp, a ternary complex between $NADP^+$, Asp, and the C(4a)-hydroperoxyflavin intermediate is formed (Scheme 2E). The primary amine of Asp performs a nucleophilic attack on the distal oxygen of the C(4a)-hydroperoxyflavin forming *N*-hydroxy-Asp, which is released

Scheme 2. Proposed Mechanism of the First Enzymatic Turnover of FzmM. Each Cycle Begins with Oxidized Enzyme (A). NADPH Binds to the Enzyme (B) and Rapidly Transfers the *pro*-R Hydrogen of the Nicotinamide Ring to the N5 Position of the FAD Moiety Forming Flavin Hydroquinone (C). Oxygen Then Reacts with the Reduced Flavin Forming a C(4a)-Hydroperoxyflavin Intermediate (D). In the Absence of Asp, this Intermediate Decays Forming Hydrogen Peroxide and Oxidized Flavin (A). When Asp is Available, the Substrate Binds (E) and Performs a Nucleophilic Attack on the Distal −OH Group of the Flavin Intermediate Forming RNH_2-OH, which is Then Released with Water (F). The Product and $NADP^+$ are Then Released, and the C(4a)-Hydroxyflavin Decays into Water and Oxidized Flavin. The Determined K_D of Asp at 7 ± 0.3 mM is Believed to be Correlated to Binding of Asp to the Hydroxy-Flavin[40,46]

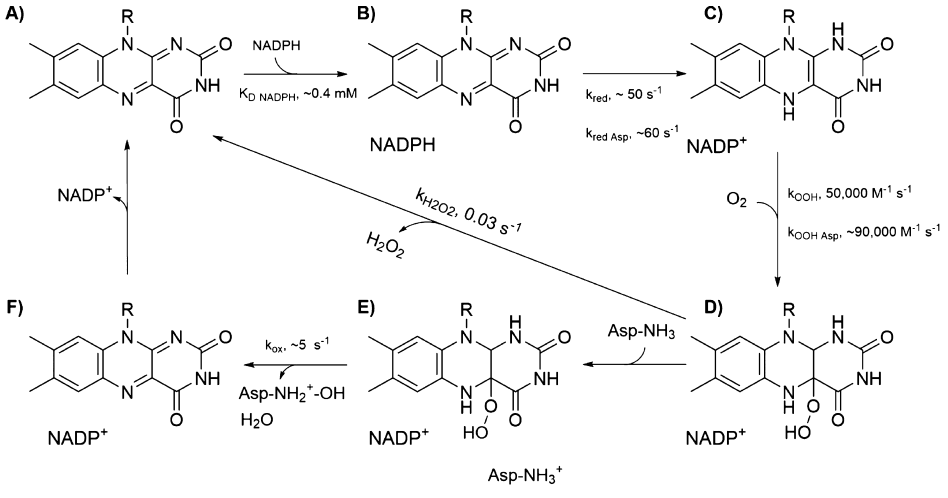

https://doi.org/10.1021/acs.biochem.1c00512
Biochemistry XXXX, XXX, XXX−XXX

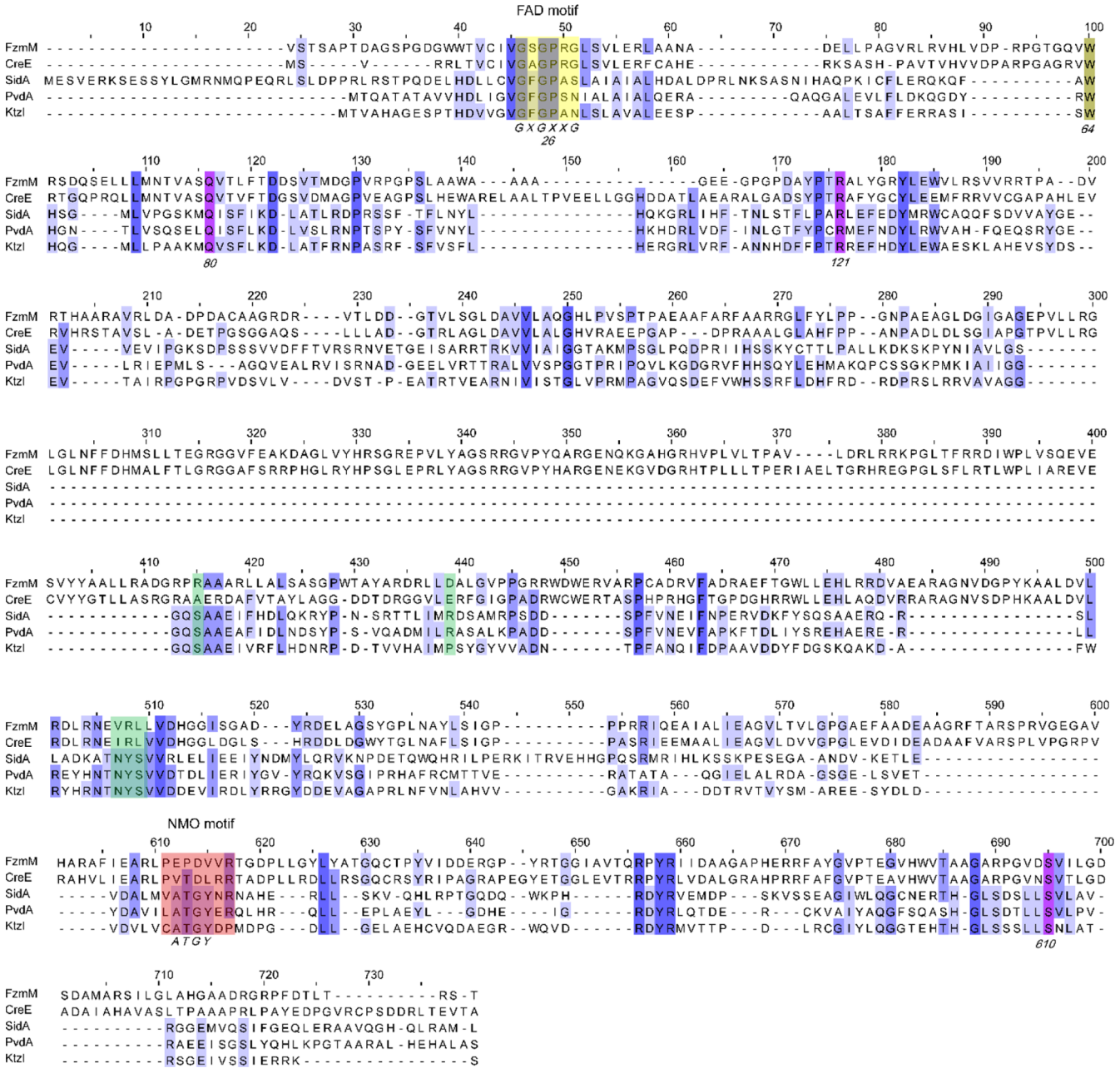

Figure 8. Sequence alignment of FzmM with its homologue from *Streptomyces cremeus* (CreE, Uniprot: A0A0K2JL70) and other NMO members. The NMOs used are L-ornithine N5 monooxygenase from *Aspergillus fumigatus* (SidA; NCBI: AAT84594.1), L-ornithine N5 monooxygenase from *Pseudomonas aeruginosa* (PvdA; Uniprot: Q51548), and L-ornithine N6 monooxygenase from *Kutzneria* sp. (Ktz; Uniprot: A8CF85). The T-Coffee server was used for the sequence alignment, and the software Jalview was used for visualization.[48,49] Residues are colored blue depending on percent identity. Residues highlighted in yellow are involved in FAD binding, green are involved in NADPH binding, pink are conserved active-site residues in SidA, and red is the "(F/V)ATGY" motif commonly found in NMOs.[14] Residues involved in FAD binding (yellow) and some active-site residues in SidA (pink) are conserved in FzmM and CreE, while residues involved in NADPH binding (green) are not. Specific residues mentioned in the discussion are numbered.

with water (Scheme 2E–F). $NADP^+$ is released, priming FzmM for a new catalytic cycle (Scheme 2F–A). Previous work has measured the accumulation of *N*-hydroxy-Asp when excess Asp was available.[18] This suggests that *N*-hydroxy-Asp is released and rebinds later for further oxidation. Rapid reaction kinetic analysis showed an increase in the k_{ox} as a function of Asp (Figure S10), with a K_D of ~7 mM, which is much higher than the K_m value. It is possible that after release of *N*-hydroxy-Asp, another Asp binds, with lower affinity, to the hydroxyflavin. Similar results were reported for SidA.[39,46]

The oligomeric states of FzmM and FzmL were determined using SEC. FzmM exists as a monomer in solution resembling PvdA (Figure S10A and Table S2)[47] where FzmL exists as a pentamer in solution (Table S2). When the enzymes were incubated together and then analyzed by SEC, both eluted separately (Figure S10). Similarly, the thermal stability of the proteins was unchanged when FzmM and FzmL were combined. These results suggest that these two enzymes do not interact or have very low affinity, and the nitrosuccinate product is transferred from FzmM to FzmL via diffusion.

https://doi.org/10.1021/acs.biochem.1c00512
Biochemistry XXXX, XXX, XXX−XXX

Several site-directed mutagenesis studies have been performed on SidA contributing to the elucidation of the structure−function relationship in this enzyme. This knowledge can provide insights into the potential function of conserved residues in FzmM. Thus, the amino acid sequences of FzmM, CreE (51% identity), SidA (15% identity), PvdA (14% identity), and KtzI (14% identity), a structural-characterized ornithine hydroxylase, were aligned to determine amino acid conservation (Figure 8). Residues R121, Q80, and S610 of FzmM were aligned to R144, Q102, and S469 of SidA, which have been shown to be associated with FAD binding or C(4a)-hydroperoxyflavin stabilization.[12,43−45] The FAD-binding motif GXGXXG and some residues that are structurally associated with FAD binding such as P26 and W64 (P49 and W90 in SidA) are also present.[16,17] Key residues involved in NADPH binding in NMOs were absent in the FzmM amino acid sequence. This includes the SidA residues: R279 which is involved in NADPH selectivity, S257 essential for $NADP^+$ orientation, the Tyr-loop which undergoes major conformational changes as a part of NADPH binding, and the signature NMO "(F/V)ATGY" motif.[11,16,42,47] The absence of these is significant as it suggests that dinucleotide substrate binding utilizes different structural features than that described in other NMOs. This could explain its unique kinetics during reduction and the multiple oxidation reaction. The residues and structures that form NADPH and Asp-binding sites remain to be identified.

FzmM was also aligned to FMO and Bayer-Villager monooxygenase (BVMO), a subclass of class B monooxygenases, to explore sequence similarities[17,50−52] (Figure S13). There was alignment of R386 and W598 in FzmM to $BVMO_{838}$ (R337 and W502), PAMO (R336 and W500), and CHMO (R329 and W492). These two residues are well-conserved in BVMOs and are essential for enzyme reduction and substrate conversion.[53−55] The conserved arginine interacts with the amide nitrogen of $NADP,^+$[53−56] while the conserved tryptophan is central in the variable "control loop" in BVMOs, which undergoes conformational changes during reduction.[52,55] We found partial alignment to the type I BVMO signature motif FXGXXXHXXXWP associated with NADPH binding (residues G207-P216 in FzmM).[53,55] When sequences sharing 48−88% identity to FzmM were aligned, this region exhibited a pattern of GLX(Y/H)XXPXNP maintaining the Gly, His, and Pro residues observed in the original motif (Figure S14). It is possible that these aligned regions serve a similar purpose in FzmM for NADPH binding as they do in BVMOs.

In summary, this report provides a detailed kinetic analysis with a focus on the first turnover performed by a nitro-forming enzyme from the NMO family. While FzmM exhibits traits characteristic of NMOs, its high reactivity with NADPH, in addition to the lack of conservation of NADPH-interacting residues, provides evidence of a structure and mechanism that differs from what has been established for other NMOs. It is of great interest to determine the structure of FzmM; however, efforts to do so have remained unsuccessful. Future studies will focus on the multiple turnovers performed by FzmM, which should provide greater mechanistic insights into this enzyme.

■ ASSOCIATED CONTENT

Supporting Information

The Supporting Information is available free of charge at https://pubs.acs.org/doi/10.1021/acs.biochem.1c00512.

KIEs in FzmM reduction, molecular mass calculated by SEC, SDS-PAGE of purification samples of FzmM, SDS-PAGE of purification samples of FzmL, UV−vis spectrum of FzmM, oxygen consumption with different substrates, Asp consumption measured by HPLC, nitrite formation with FzmM and FzmL, FzmM reduction with NADH, observed rates at 370 and 450 nm during oxidation, oxidation at increasing concentrations of Asp, SEC chromatograms of FzmM and FzmL, FzmM thermal shift with different reducing agents, pH profile on FzmM, sequence alignment of FzmM to BVMOs, and sequence alignment of FzmM to putative NMOs (PDF)

Accession Codes

FzmM protein, WP_053787792 (NCBI); FzmL, WP_053787793 (NCBI). Accession codes for proteins mentioned in the discussion are provided in the figure legends of Figures 8, S13, and S14.

■ AUTHOR INFORMATION

Corresponding Author

Pablo Sobrado − *Department of Biochemistry and Center for Drug Discovery, Virginia Tech, Blacksburg, Virginia 24061, United States;* orcid.org/0000-0003-1494-5382; Email: psobrado@vt.edu

Author

Hannah Valentino − *Department of Biochemistry and Center for Drug Discovery, Virginia Tech, Blacksburg, Virginia 24061, United States;* Present Address: Oak Ridge National Laboratory, Biosciences Division, Oak Ridge, TN 378, United States

Complete contact information is available at: https://pubs.acs.org/10.1021/acs.biochem.1c00512

Author Contributions

H.V.: data curation; H.V. and P.S.: conceptualization, formal analysis, writing-original draft review, and editing; and P.S.: funding acquisition and project administration.

Funding

Research reported in this publication was supported by the National Science Foundation [grant CHE 2003658 (to P.S.)]. H.V. was supported by the ICTAS Scholar Fellowship.

Notes

The authors declare no competing financial interest.

■ REFERENCES

(1) Walsh, C. T.; Wencewicz, T. A. Flavoenzymes: Versatile catalysts in biosynthetic pathways. *Flavoenzymes: Versatile Catalysts in Biosynthetic Pathways*; The Royal Society of Chemistry, 2013; Vol. *30*, pp 175−200.

(2) Teufel, R. Flavin-catalyzed redox tailoring reactions in natural product biosynthesis. *Arch. Biochem. Biophys.* **2017**, *632*, 20−27.

(3) Huijbers, M. M. E.; Montersino, S.; Westphal, A. H.; Tischler, D.; van Berkel, W. J. H. Flavin dependent monooxygenases. *Arch. Biochem. Biophys.* **2014**, *544*, 2−17.

(4) Chocklett, S. W.; Sobrado, P. Aspergillus fumigatus SidA is a highly specific ornithine hydroxylase with bound flavin cofactor. *Biochemistry* **2010**, *49*, 6777−6783.

(5) Robinson, R. M.; Sobrado, P. *Flavin-Dependent Monooxygenases in Siderophore Biosynthesis*; Hille, R., Miller, S., Palfey, B., Eds.; De Gruyter, 2013.

(6) Abdelwahab, H.; Robinson, R.; Rodriguez, P.; Adly, C.; El-Sohaimy, S.; Sobrado, P. Identification of structural determinants of NAD (P) H selectivity and lysine binding in lysine N6-monooxygenase. *Arch. Biochem. Biophys.* **2016**, *606*, 180−188.
(7) Binda, C.; Robinson, R. M.; Martin del Campo, J. S.; Keul, N. D.; Rodriguez, P. J.; Robinson, H. H.; Mattevi, A.; Sobrado, P. An unprecedented NADPH domain conformation in lysine monooxygenase NbtG provides insights into uncoupling of oxygen consumption from substrate hydroxylation. *J. Biol. Chem.* **2015**, *290*, 12676−12688.
(8) Li, H.; Forson, B.; Eckshtain-Levi, M.; Valentino, H.; Martín del Campo, J. S.; Tanner, J. J.; Sobrado, P. Biochemical Characterization of the Two-Component Flavin-Dependent Monooxygenase Involved in Valanimycin Biosynthesis. *Biochemistry* **2020**, *60*, 31−40.
(9) Hofmann, M.; Martin del Campo, J. S.; Sobrado, P.; Tischler, D. Biosynthesis of desferrioxamine siderophores initiated by decarboxylases: a functional investigation of two lysine/ornithine-decarboxylases from *Gordonia rubripertincta* CWB2 and *Pimelobacter simplex* 3E. *Arch. Biochem. Biophys.* **2020**, *689*, 108429.
(10) Campbell, A. C.; Robinson, R.; Mena-Aguilar, D.; Sobrado, P.; Tanner, J. J. Structural determinants of flavin dynamics in a class B monooxygenase. *Biochemistry* **2020**, *59*, 4609−4616.
(11) Campbell, A. C.; Stiers, K. M.; Martin del Campo, J. S.; Mehra-Chaudhary, R.; Sobrado, P.; Tanner, J. J. Trapping conformational states of a flavin-dependent N-monooxygenase in crystallo reveals protein and flavin dynamics. *J. Biol. Chem.* **2020**, *295*, 13239−13249.
(12) Franceschini, S.; Fedkenheuer, M.; Vogelaar, N. J.; Robinson, H. H.; Sobrado, P.; Mattevi, A. Structural Insight into the Mechanism of Oxygen Activation and Substrate Selectivity of Flavin-Dependent N-Hydroxylating Monooxygenases. *Biochemistry* **2012**, *51*, 7043−7045.
(13) Mügge, C.; Heine, T.; Baraibar, A. G.; van Berkel, W. J. H.; Paul, C. E.; Tischler, D. Flavin-dependent N-hydroxylating enzymes: distribution and application. *Appl. Microbiol. Biotechnol.* **2020**, *104*, 6481−6499.
(14) Meneely, K. M.; Lamb, A. L. Biochemical characterization of a flavin adenine dinucleotide-dependent monooxygenase, ornithine hydroxylase from *Pseudomonas aeruginosa*, suggests a novel reaction mechanism. *Biochemistry* **2007**, *46*, 11930−11937.
(15) Meneely, K. M.; Barr, E. W.; Bollinger, J. M.; Lamb, A. L. Kinetic mechanism of ornithine hydroxylase (PvdA) from *Pseudomonas aeruginosa*: substrate triggering of O2 addition but not flavin reduction. *Biochemistry* **2009**, *48*, 4371−4376.
(16) Olucha, J.; Lamb, A. L. Mechanistic and structural studies of the N-hydroxylating flavoprotein monooxygenases. *Bioorg. Chem.* **2011**, *39*, 171−177.
(17) Olucha, J.; Meneely, K. M.; Chilton, A. S.; Lamb, A. L. Two structures of an N-hydroxylating flavoprotein monooxygenase ornithine hydroxylase from *Pseudomonas aerugionosa*. *J. Biol. Chem.* **2011**, *286*, 31789−31798.
(18) Huang, Z.; Wang, K.-K. A.; van der Donk, W. A. New Insights into the Biosynthesis of Fosfazinomycin. *Chem. Sci.* **2016**, *7*, 5219−5223.
(19) Huang, Z.; Wang, K.-K. A.; Lee, J.; van der Donk, W. A. Biosynthesis of fosfazinomycin is a convergent process. *Chem. Sci.* **2015**, *6*, 1282−1287.
(20) Gao, J.; Ju, K.-S.; Yu, X.; Velásquez, J. E.; Mukherjee, S.; Lee, J.; Zhao, C.; Evans, B. S.; Doroghazi, J. R.; Metcalf, W. W.; van der Donk, W. A. Use of a phosphonate methyltransferase in the identification of the fosfazinomycin biosynthetic gene cluster. *Angew. Chem., Int. Ed.* **2014**, *53*, 1334−1337.
(21) Sugai, Y.; Katsuyama, Y.; Ohnishi, Y. A nitrous acid biosynthetic pathway for diazo group formation in bacteria. *Nat. Chem. Biol.* **2016**, *12*, 73−75.
(22) Waldman, A. J.; Pechersky, Y.; Wang, P.; Wang, J. X.; Balskus, E. P. The cremeomycin biosynthetic gene cluster encodes a pathway for diazo formation. *ChemBioChem* **2015**, *16*, 2172−2175.
(23) Markofsky, S. B. *Nitro compounds, alphatic*; Wiley-VCH Verlag GmbH and Co.31.KGaA.1, 2000.
(24) Badgujar, D. M.; Talawar, M. B.; Mahulikar, P. P. Review on greener and safer synthesis of nitro compounds. *Propellants, Explos., Pyrotech.* **2016**, *41*, 24−34.
(25) [dataset] Environmental Protection Agency. *CDR National Aggregate Production Volume*; Environmental Protection Agency. Chem IDs: 75525, 108032, 79243, 79469, 98953, 2016.
(26) Ballini, R.; Palmieri, A. Synthetic procedures for the preparation of nitroalkanes. *Adv. Synth. Catal.* **2018**, *360*, 2240−2266.
(27) Kuchurov, I. V.; Zharkov, M. N.; Fershtat, L. L.; Makhova, N. N.; Zlotin, S. G. Prospective symbiosis of green chemistry and energetic materials. *ChemSusChem* **2017**, *10*, 3914−3946.
(28) Kong, M.; Wang, K.; Dong, R.; Gao, H. Enzyme catalytic nitration of aromatic compounds. *Enzyme Microb. Technol.* **2015**, *73−74*, 34−43.
(29) Hollmann, F.; Arends, I. W. C. E.; Buehler, K.; Schallmey, A.; Bühler, B. Enzyme-mediated oxidations for the chemist. *Green Chem.* **2011**, *13*, 226−265.
(30) Waldman, A. J.; Ng, T. L.; Wang, P.; Balskus, E. P. Heteroatom−heteroatom bond formation in natural product biosynthesis. *Chem. Rev.* **2017**, *117*, 5784−5863.
(31) Gunji, S.; Arima, K.; Beppu, T. Screening of antifungal antibiotic according to activities inducing morphological abnormalities. *Agric. Biol. Chem.* **1983**, *47*, 2061−2069.
(32) Ogita, T.; Gunji, S.; Fukazawa, Y.; Terahara, A.; Kinoshita, T.; Nagaki, H.; Beppu, T. The structures of fosfazinomycins A and B. *Tetrahedron* **1983**, *24*, 2283−2286.
(33) Waldman, A. J.; Balskus, E. P. Discovery of a diazo-forming enzyme in cremeomycin biosynthesis. *J. Org. Chem.* **2018**, *83*, 7539−7546.
(34) Wang, K. K. A.; Ng, T. L.; Wang, P.; Huang, Z.; Balskus, E. P.; van der Donk, W. A. Glutamic acid is a carrier for hydrazine during the biosyntheses of fosfazinomycin and kinamycin. *Nat. Commun.* **2018**, *9*, 1−11.
(35) Dhatwalia, R.; Singh, H.; Solano, L. M.; Oppenheimer, M.; Robinson, R. M.; Ellerbrock, J. F.; Sobrado, P.; Tanner, J. J. Identification of the NAD (P) H binding site of eukaryotic UDP-galactopyranose mutase. *J. Am. Chem. Soc.* **2012**, *134*, 18132−18138.
(36) Fabiani, A.; Versari, A.; Parpinello, G. P.; Castellari, M.; Galassi, S. High-performance liquid chromatographic analysis of free amino acids in fruit juices using derivatization with 9-fluorenylmethyl-chloroformate. *J. Chromatogr. Sci.* **2002**, *40*, 14−18.
(37) Huynh, K.; Partch, C. L. Analysis of protein stability and ligand interactions by thermal shift assay. *Curr. Protoc. Protein Sci.* **2015**, *79*, 28.9.1−28.9.14.
(38) Valentino, H.; Sobrado, P. Performing anaerobic stopped-flow spectrophotometry inside of an anaerobic chamber. *Methods Enzymol.* **2019**, *620*, 51−88.
(39) Romero, E.; Gómez Castellanos, J. R.; Gadda, G.; Fraaije, M. W.; Mattevi, A. Same substrate, many reactions: oxygen Activation in flavoenzymes. *Chem. Rev.* **2018**, *118*, 1742−1769.
(40) Mayfield, J. A.; Frederick, R. E.; Streit, B. R.; Wencewicz, T. A.; Ballou, D. P.; DuBois, J. L. Comprehensive spectroscopic, steady state, and transient kinetic studies of a representative siderophore-associated flavin monooxygenase. *J. Biol. Chem.* **2010**, *285*, 30375−30388.
(41) Romero, E.; Fedkenheuer, M.; Chocklett, S. W.; Qi, J.; Oppenheimer, M.; Sobrado, P. Dual role of NADP(H) in the reaction of a flavin dependent N-hydroxylating monooxygenase. *Biochim. Biophys. Acta, Proteins Proteomics* **2012**, *1824*, 850−857.
(42) Robinson, R.; Franceschini, S.; Fedkenheuer, M.; Rodriguez, P. J.; Ellerbrock, J.; Romero, E.; Echandi, M. P.; Martin Del Campo, J. S.; Sobrado, P. Arg279 is the key regulator of coenzyme selectivity in the flavin-dependent ornithine monooxygenase SidA. *Biochim. Biophys. Acta* **2014**, *1844*, 778−784.
(43) Robinson, R. M.; Klancher, C. A.; Rodriguez, P. J.; Sobrado, P. Flavin oxidation in flavin-dependent N monooxygenases. *Protein Sci.* **2018**, *28*, 90−99.
(44) Robinson, R.; Qureshi, I. A.; Klancher, C. A.; Rodriguez, P. J.; Tanner, J. J.; Sobrado, P. Contribution to catalysis of ornithine

https://doi.org/10.1021/acs.biochem.1c00512
Biochemistry XXXX, XXX, XXX−XXX

binding residues in ornithine N5-monooxygenase. *Arch. Biochem. Biophys.* **2015**, *585*, 25−31.
(45) Badieyan, S.; Bach, R. D.; Sobrado, P. Mechanism of N-hydroxylation catalyzed by flavin-dependent monooxygenases. *J. Org. Chem.* **2015**, *80*, 2139−2147.
(46) Sobrado, P. Flavin-Dependent *N*-Hydroxylating monooxygenases in Bacterial and Fungi Siderophore Biosynthesis. In *Flavins and Flavoproteins*; Miller, S., Hille, R., Palfey, B., Eds.; Lulu: Raleigh, NC, 2013; pp 265−276.
(47) Shirey, C.; Badieyan, S.; Sobrado, P. Role of Ser-257 in the sliding mechanism of NADP (H) in the reaction catalyzed by the *Aspergillus fumigatus* flavin-dependent ornithine N5-monooxygenase SidA. *J. Biol. Chem.* **2013**, *288*, 32440−32448.
(48) Waterhouse, A. M.; Procter, J. B.; Martin, D. M. A.; Clamp, M.; Barton, G. J. Jalview Version 2 - a multiple sequence alignment editor and analysis workbench. *Bioinformatics* **2009**, *25*, 1189−1191.
(49) Notredame, C.; Higgins, D. G.; Heringa, J. T-Coffee: A novel method for fast and accurate multiple sequence alignment. *J. Mol. Biol.* **2000**, *302*, 205−217.
(50) Ferroni, F. M.; Tolmie, C.; Smit, M. S.; Opperman, D. J. Structural and catalytic characterization of a fungal Baeyer-Villiger monooxygenase. *PLoS One* **2016**, *11*, No. e0160186.
(51) Malito, E.; Alfieri, A.; Fraaije, M. W.; Mattevi, A. Crystal structure of a Baeyer−Villiger monooxygenase. *Proc. Natl. Acad. Sci. U. S. A.* **2004**, *101*, 13157−13162.
(52) Mirza, I. A.; Yachnin, B. J.; Wang, S.; Grosse, S.; Bergeron, H.; Imura, A.; Iwaki, H.; Hasegawa, Y.; Lau, P. C. K.; Berghuis, A. M. Crystal structures of cyclohexanone monooxygenase reveal complex domain movements and a sliding cofactor. *J. Am. Chem. Soc.* **2009**, *131*, 8848−8854.
(53) Leisch, H.; Morley, K.; Lau, P. C. K. Baeyer−Villiger monooxygenases: more than just green chemistry. *Chem. Rev.* **2011**, *111*, 4165−4222.
(54) Fürst, M. J. L. J.; Gran-Scheuch, A.; Aalbers, F. S.; Fraaije, M. W. Baeyer−Villiger monooxygenases: tunable oxidative biocatalysts. *ACS Catal.* **2019**, *9*, 11207−11241.
(55) Fürst, M. J.; Fiorentini, F.; Fraaije, M. W. Beyond active site residues: overall structural dynamics control catalysis in flavin-containing and heme-containing monooxygenases. *Struct. Biol* **2019**, *59*, 29−37.
(56) Torres Pazmiño, D. E.; Baas, B.-J.; Janssen, D. B.; Fraaije, M. W. Kinetic Mechanism of Phenylacetone Monooxygenase from *Thermobifida fusca*. *Biochemistry* **2008**, *47*, 4082−4093.

https://doi.org/10.1021/acs.biochem.1c00512
Biochemistry XXXX, XXX, XXX−XXX